Acta Geologica Sinica (English Edition), 2020, 94(1): 176–188

Typical Soft–Sediment Deformation Structures Induced by Freeze/Thaw Cycles: A Case Study of Quaternary Alluvial Deposits in the Northern Qiangtang Basin, Tibetan Plateau

ZHONG Ning[1, 2, 3], LI Haibing[1, 2, *], JIANG Hanchao[4], LU Haijian[1, 2], ZHENG Yong[1, 2], HAN Shuai[1, 2] and YE Jiachan[1, 2]

[1] *Key Laboratory of Deep–Earth Dynamics, Ministry of Natural Resources, Beijing 100037, China*
[2] *Institute of Geology, Chinese Academy of Geological Sciences, Beijing 100037, China*
[3] *Institute of Geomechanics, Chinese Academy of Geological Sciences, Beijing, 100081, China*
[4] *State Key Laboratory of Earthquake Dynamics, Institute of Geology, China Earthquake Administration, Beijing 100029, China*

Abstract: With the objective of establishing a distinction between deformation structures caused by freeze/thaw cycles and those resulting from seismic activity, we studied three well–exposed alluvial deposits in a section at Dogai Coring, northern Qiangtang Basin, Tibetan Plateau. Deformation is present in the form of plastic structures (diapirs, folds and clastic dykes), brittle structures (micro–faults) and cryogenic wedges. These soft–sediment deformation features (except the micro–faults) are mainly characterized by meter–scale, non–interlayered, low–speed and low–pressure displacements within soft sediments, most commonly in the form of plastic deformation. Taking into account the geographic setting, lithology and deformation features, we interpret these soft–sediment deformation features as the products of freeze/thaw cycles, rather than of earthquake–induced shock waves, thus reflecting regional temperature changes and fluctuations of hydrothermal conditions in the uppermost sediments. The micro–faults (close to linear hot springs) are ascribed to regional fault activity; however, we were unable to identify the nature of the micro–faults, perhaps due to disturbance by subsequent freeze/thaw cycles. This study may serve as a guide to recognizing the differences between deformation structures attributed to freeze/thaw cycles and seismic processes.

Key words: soft–sediment deformation structures, freeze/thaw cycles, Dogai Coring, Qiangtang Basin

Citation: Zhong et al., 2020. Typical Soft–Sediment Deformation Structures Induced by Freeze/Thaw Cycles: A Case Study of Quaternary Alluvial Deposits in the Northern Qiangtang Basin, Tibetan Plateau. Acta Geologica Sinica (English Edition), 94(1): 176–188. DOI: 10.1111/1755-6724.14345

1 Introduction

Soft–sediment deformation structures (SSDS) are caused by liquefaction and/or fluidization during the deformation of water–saturated unconsolidated sediments at the top of a sedimentary sequence, and may be associated with various natural processes (Owen, 1987; Qiao et al., 2017; Zhong et al., 2017, 2020). These processes can be triggered by many more processes, such as earthquakes (Obermeier, 1996; Wang et al., 2011; Owen and Moretti, 2011; Li et al., 2012; Tian et al., 2013, 2016; He and Qiao, 2015; Jiang et al., 2016; Qiao et al., 2017; Zhong, 2017; Zhong et al., 2017, 2019; Liang et al., 2018; Zhong et al., 2018), rapid sedimentation (Lowe, 1975; Postma, 1983), groundwater movement (Owen, 1996; Massari et al., 2001; Ravier et al., 2014), storm–induced currents (Molina et al., 1998; Alfaro et al., 2002), gravity flows (Owen and Moretti, 2008; Yang et al., 2017) or slumping (Ge et al., 2015) and freeze/thaw cycles (Vandenberghe,1988,1992; Murton, 2001; Giles et al., 2013). SSDS triggered by earthquakes can take various forms and are frequently discussed, especially in tectonically affected areas (Qiao et al., 2017). Therefore, the seismogenic interpretation of SSDS is somewhat expanding. Nevertheless, this interpretation can be problematic, as seismically–induced SSDS are not fundamentally different (e.g. with respect to type and deformation mechanism) from non–seismic SSDS. Moreover, a specific deformational process can result in different types of SSDS, where a specific type of SSDS (e.g. diapir structures) can be formed by strongly different deformational mechanisms (e.g. liquefaction or fluidization, thixotropic processes, gravity). Unfortunately, few studies have critically assessed whether deformation structures had a seismic or non–seismic trigger (Van Loon and Brodzikowski, 1987; Greb and Archer, 2007; Zhong, 2017).

Freeze/thaw cycles, as present particularly under periglacial conditions, is another effective mechanism that can cause SSDS (Vandenberghe, 1988, 2016; Murton, 2001; Superson et al., 2010; Wang et al., 2013; Jin et al., 2016; Giles et al., 2017). In this case, the deformation mechanism includes cryostatic pressure, gravitational loading of sediments with reversed density gradient and

* Corresponding author. E-mail: lihaibing06@163.com

thermokarst (Superson et al., 2010). Owing to increasing pore water pressure in active layers, the unfrozen and fluidized sediment–water mixture may be expelled by hydrostatic pressure into places of lesser resistance (Vandenberghe, 2007). Freeze/thaw cycles can also cause liquefaction and/or fluidization. A classification scheme that assigns the wide range of cryoturbation structures to six morphological types (undulations or individual folds, symmetrical or intensely folded forms, drop-like and pocket-like structures, diapirs or flame-like, dykes, irregular contortion structures) has been proposed by Vandenberghe (1988). Cryogenic wedges are the most common and typical deformation structure in periglacial environments (Vandenberghe, 1988; Jin et al., 2016), and are often used as direct evidence of freeze/thaw cycles. Much attention has consequently been paid to the criteria used to recognize SSDS caused by freeze/thaw cycles (Vandenberghe, 1988, 1992; van Vliet–Lanoë et al., 2004; Vandenberghe et al., 2016; Petera–Zganiacz and Dzieduszyńska, 2017), but few studies have compared SSDS due to seismic activity with those due to freeze/thaw cycles.

The Qiangtang Basin, with an average elevation of 4800 m (Fig. 1a), has the lowest annual average surface temperature and forms the most extensive permafrost area on the Tibetan Plateau (TP) (Wang et al., 2008). Therefore, freeze/thaw cycles are common; they result in frost weathering, cryoturbation and a large variety of SSDS (Vandenberghe, 2004; Wang et al., 2013). To the present study deals with late Quaternary alluvial deposits of the Dogai Coring (DC) section in the northern Qiangtang Basin, Tibetan Plateau. The objectives are (1) to interpret the deformation and trigger mechanisms of the various types of SSDS, (2) to develop key criteria to distinguish between deformation structures induced by freeze/thaw cycles and those triggered by seismic activity, and (3) to improve our understanding of the tectonic activity and environmental implications for the area.

2 Geographic and Geological Setting

The DC section is located south of Dogai Coring (Fig. 2a). It includes three sections with late Quaternary alluvial deposits: sections DC–2 and DC–3 form the T1 terrace of the Changshui River, and section DC–1 forms the T1 terrace of a former river (Fig. 1b and Fig. 2a). The area is composed of low mountains, hills and lakes; the average elevation is about 5,000 meters, and relative height is generally between 200–1000 meters (Chen, 2012). The 35 years (1966–2010) meteorological data from Naqu show an annual average temperature of –1.5–1.8°C, mean 0.1°C (Lin et al., 2012). The average monthly temperatures over 40 years (1961–2000) are higher than 0 °C from May to September, with the remainder below 0 °C (Mao et al., 2007). Mountain summits have perennial snow cover, forming glaciers. Cryoturbation often occurs in loose deposits on the slopes (Fig. 2c, 2d).

The bedrock in the study area consists of Jurassic limestones and bioclastic limestones, Eocene sandstones, mudstones, and glutenous rocks (Fig. 1b, Ren et al., 2015). Large–scale faulting and intense folding characterizes the Mesozoic strata of the Qiangtang Basin, leading to the exposure of Mesozoic and Paleozoic or even older formations at the present day surface (Wang et al., 2006). The neotectonic movement is dominated by faults and mud volcanic activity (Li et al., 1998; Yang et al., 2009; Ratschbacher et al., 2011). Quaternary deposits such as alluvial fans, river terraces and slope wash are distributed

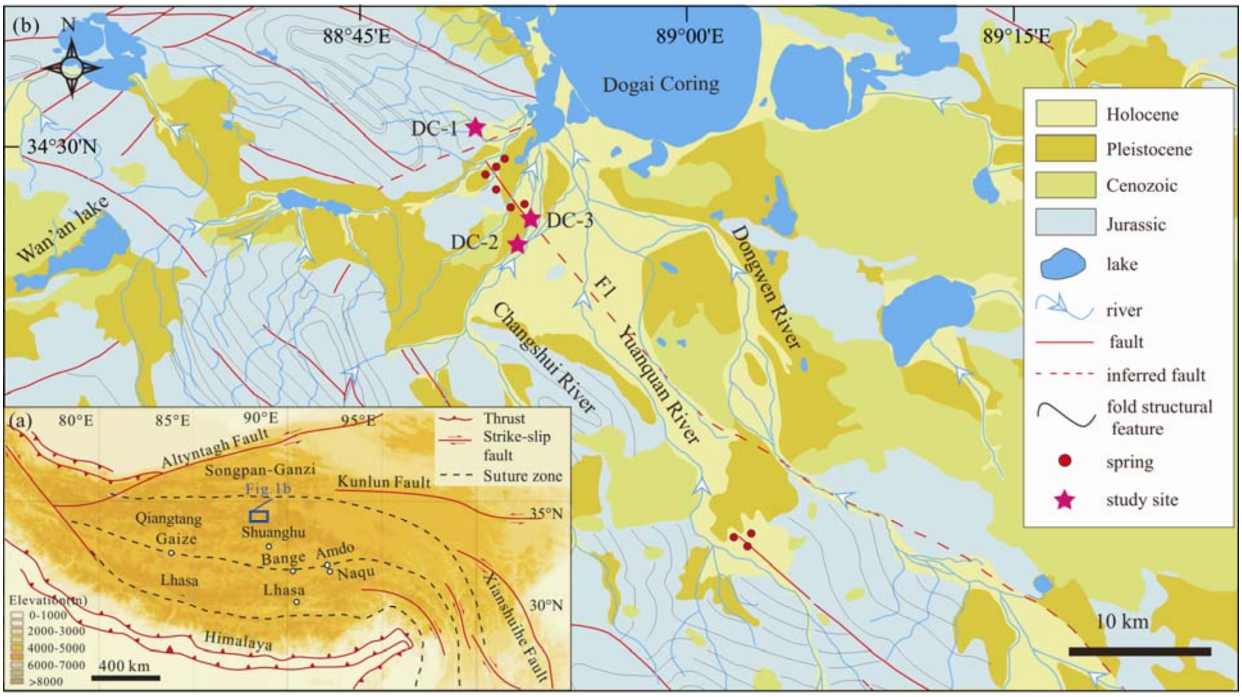

Fig. 1. (a) Topographic map and major tectonic units of the Tibetan–Himalayan orogen (Li et al., 2015), and location of the study area (pink rectangle); (b) geological map of the study area and the location of the Dogai Coring section (modified from the 1:250000 Dogai Coring geological map, Chengdu Institute of Geology and Mineral Resources, 2005).

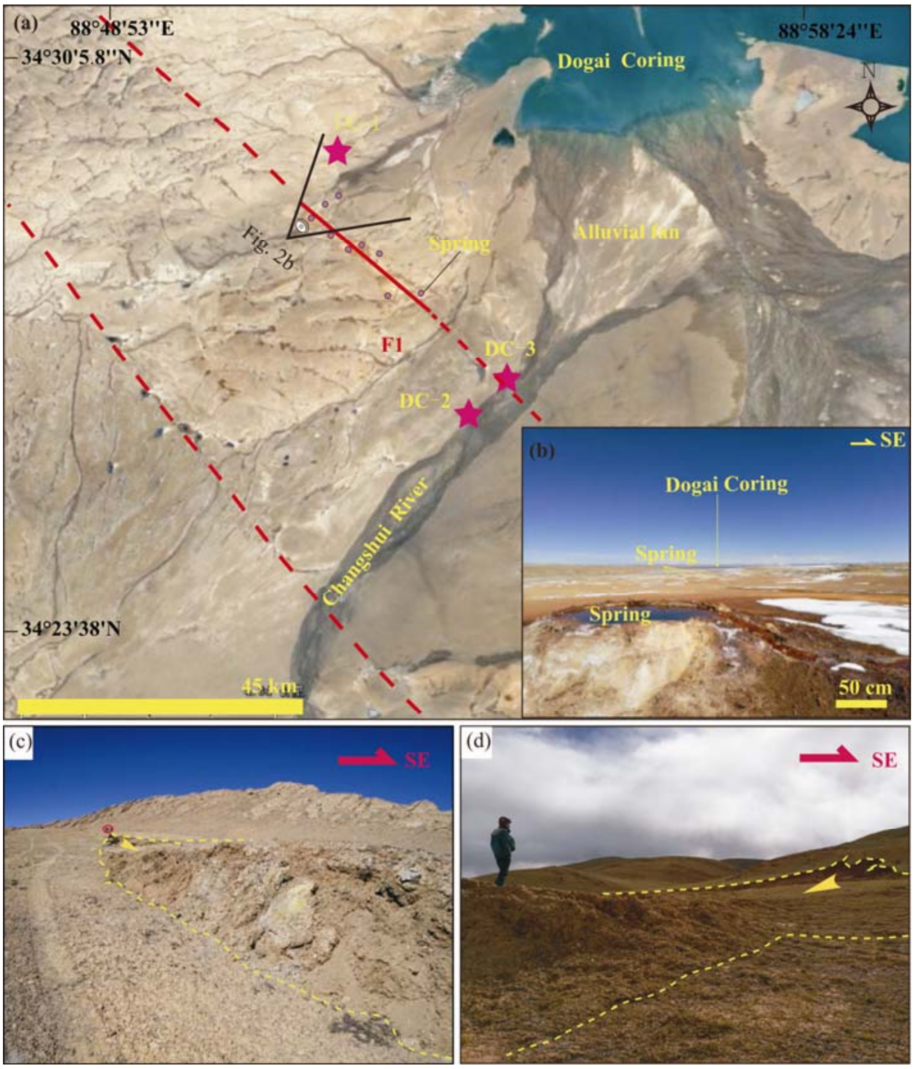

Fig. 2. (a) Interpreted map from Google Earth showing the regional landscape; (b) photographs of travertine mound and spring outcrop in field; (c-d) cryoturbation terrain (34° 02'44.07"N, 88°30'58.72"E, 5035 m a.s.l and 34°17'27.19", 88°16'28.30", 5225 m a.s.l.).

mainly along the river and its tributaries, and the layers of river terrace sediments generally exhibit varying degrees of deformation. A series of depositing travertine domes and springs is present on the south bank of Dogai Coring, mainly along the F1 fault (Fig. 2b).

3 Lithology

The well–exposed DC profile (Fig. 3) includes three sections (DC–1, DC–2 and DC–3), with thicknesses of 2.7 m, 6 m and 5.5 m, respectively. The lithology primarily comprises light yellow sand, clayey silt, and dark gray gravel. DC–1 at 0–20 cm is brown soil with massive structure; 20–95 cm is dark gray gravel with light yellow sand and clayey silt; 95–270 cm is light yellow sand with clayey silt, with parallel bedding. Gravels are poorly mixed, poorly sorted, matrix supported and largely composed of limestone. DC–2 and DC–3 show a similar stratigraphy. Sand and clayey silt lenses are visible in DC–2 and DC–3 (Fig. 3).

4 Morphological Features of the SSDS

4.1 Cryogenic wedges

Cryogenic wedges are common deformation structures within permafrost, and have been reported from the Grubbenvorts, southern Netherlands (Vandenberghe, 1992); Tuktoyaktuk Coastlands, western Arctic Canada (Murton, 2001), Inner Mongolia, China (Vandenberghe et al., 2004); the Landes region, southwestern France (Bertran et al., 2010); the Miechów Upland, Poland (Pawelec et al., 2015) and the Yilijiqi-Wuma River in the northern Da Xing’anling Mountains, Northeast China (Jin et al., 2016). According to their different filling materials, cryogenic wedge structures can be further divided into ice wedge and primary gravel, sand or soil wedge (Jin et al., 2016). The cryogenic wedges are vertically foliated and characteristically wedge-shaped bodies of ground (Harry and Gozdzik, 1988). The DC section contains soil wedges (Figs. 3, 4c) and sand wedges (Fig. 7), located in the upper part of the three sections. Soil wedges are located on the

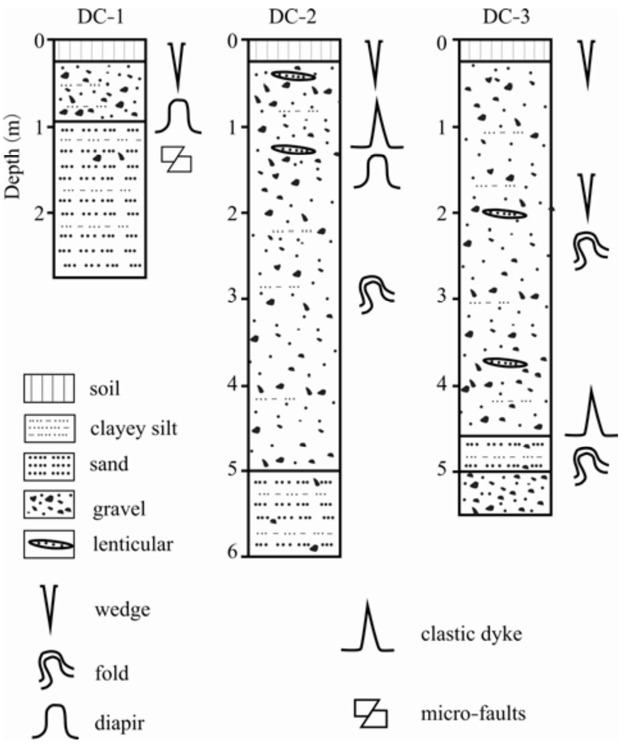

Fig. 3. Simplified lithological column of the Dogai Coring (DC) alluvial deposits section, showing the positions of SSD layers.

surface, and wedge into the underlying gravel layer or sand layer with sharp edges. A typical soil wedge structure is 0.3–0.5 m wide and 0.4–0.8 m high. Sand wedges are composed of sand to gravel that intrudes into underlying gravel beds. Their deformation scale is larger; a typical sand wedges structure is 1.5 m wide and 1 m high. This typical feature has a wide top, narrow bottom, sharp edges and corners, and gradually decreases in size downwards.

4.2 Diapirs

Diapirs or flame-like structures are formed by the upwards movement of unconsolidated deposits caused by cryohydrostatic or pore pressure (Vandenberghe, 1988, 1992; Qiao et al., 2017). Simple diapirs are observed in the DC–1 section at depths of 0.2–1.7 m, occurring as light–yellow sand and clayey silt intruding slowly upwards or laterally into the overlying gravel and brown soil layer (Fig. 4). The deformed layer contains some small gravel, with lithology that is consistent with the overlying gravel layer. Obvious cracks in the middle of the section may be related to the latest freeze/thaw cycles. A typical diapir structure is 2–3 m wide and 0.9–1.8 m high. Liquefied diapirs are also observed in the DC–2 section at depths of 1.2–2.8 m (Fig. 6). They occur as the light–yellow sand and clayey silt slowly intruding into the overlying gravel layer, with lateral flow and deformation. The top of the deformed layer contains more gravel, but the boundary with the bedding is increasingly blurred, perhaps reflecting a gradual reduction in deformation intensity. A typical liquefied diapir structure is 1–2 m wide and 1–1.6 m high.

Similar deformation structures have been described at Beerse, Belgium (Vandenberghe, 1992); the Middle Pleistocene (Anglian) Barham Soil, eastern England (Murton et al., 1995); the Wisłok Valley, Southeast Poland (Superson et al., 2010); at the interface between the Menyuan Basin and the Qilian Mountains, northeastern TP (Wang et al., 2013) and Central Poland (Petera-Zganiacz and Dzieduszyńska, 2017).

4.3 Micro–faults

The DC–1 section contains a micro–fault at depths of 1.0–1.7 m, comprising a high–angle planar fault that affected beds thicker than ~70 cm, with offsets of ~20 cm (Fig. 5). Micro-faults have been seen elsewhere, such as at Diaolin (Xu et al., 2015); Shawan (Zhong et al., 2019) and in the Lixian lacustrine sections (Jiang et al., 2016) in the eastern TP; the Tamuchage Depression in Mongolia (Wang et al., 2008); the Bajo Segura Basin in Spain (Alfaro et al., 2001) and at Vens Lake in France (Petersen et al., 2014).We note that (1) the fault in Fig. 5 must be a synsedimentary feature (the fault disappears upwards, and is overlain by undisturbed levels) that developed during a stage of brittle deformation; (2) the DC–1 section is located on the F1 fault, and there are a series of depositing travertine domes and springs along the F1 fault (Niu et al., 2014); and (3) there is no evidence of gravitational slides. Although micro–faults are seen in a variety of strata with diverse tectonic settings, in all cases they are interpreted as consequence of seismic activity. Interestingly, the strata on both sides of the micro–fault cannot be compared; the upper and lower parts are reversed and normal, respectively. We assume that the displacement of sediment particles may have been caused by the compressive stress of volume expansion during freezing and gravity collapse during thawing. Along the fault plane, there is a sand dyke with a wide bottom and narrow top, which have been caused by sand injection into the frost fissures.

4.4 Fold structures

Fold structures are observed in the DC–2 and DC–3 sections, at depths of 2.0–3.8 m and 0.9–5.1 m, respectively (Figs.7–9). These were induced by vertical and lateral forces which squeezed out the soft sediment sideways and upwards, causing it to fold into diapirs of various shapes (Vandenberghe, 1988; Superson et al., 2010). We can identify two types of fold (recumbent fold and irregular fold) based on their morphology, which are overlain and underlain by gravel beds. Recumbent folds are well developed in the DC section (Figs.7, 9, 10); they form when the sand and clayey silt layer or gravel layer are squeezed and wrinkled, then subjected to the compressive stress of the gravitational loading, forming a recumbent shape. The wings of the fold are relatively symmetrical. Interestingly, the fold–axis orientation fluctuates, but is mostly parallel to the stratum. A typical recumbent fold structure is 2–3 m wide and 0.6–1 m high. The DC–3 section contains an irregular fold at depths of 4.4–5.1 m (Fig. 8), in a light–yellow clayey silt layer with parallel bedding. The deformation structure is 1.1 m wide and 0.7 m high. Irregular folds are also observed in the DC –3 section at depths of 1–3 m (Fig. 9), occurring where the

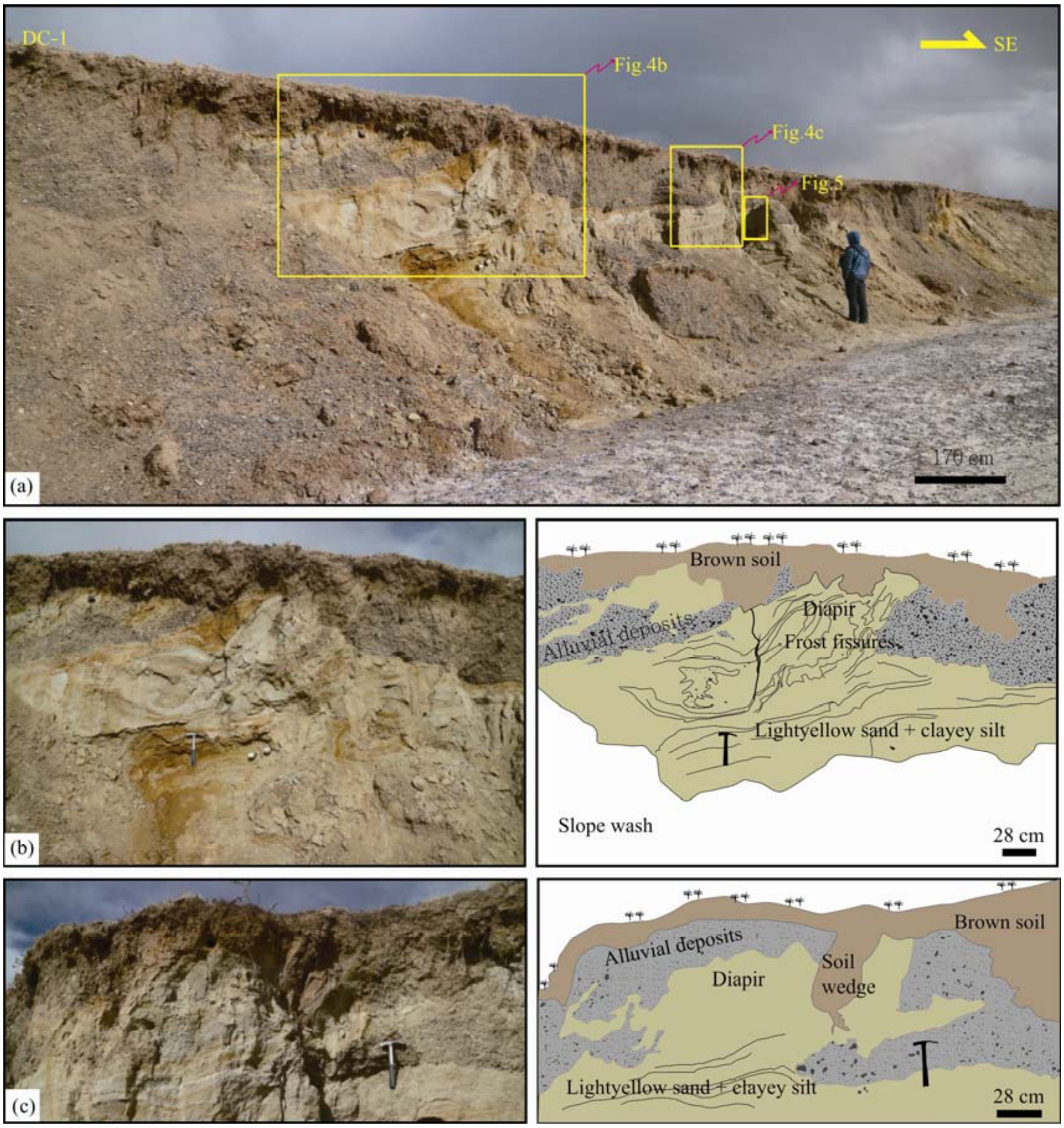

Fig. 4. Soil wedges and diapir structures in the DC–1 alluvial deposits section.
(a) Location and distribution of SSDS in the DC-1 profile. Person (170 cm high) for scale; (b) light yellow sand and clayey silt (weak bedding) intrude into the overlying gravel layer and the brown soil layer, forming diapirs. Note the frost fissures in diapir structures; (c) the brown soil layer has collapsed under gravity and piles up to form soil wedges. Hammer (28 cm long) for scale.

sand layer or gravel layer became squeezed and wrinkled. The angle between the axial plane of the fold and the sedimentary surface is 30°–45°. The deformation structure is typically 2–3.5 m wide and 1.5–2 m high.

Similar deformational structures have been described in the synrift Escucha Formation (late Aptian–middle Albian) in Teruel, Spain (Rodríguez-López et al., 2007); the Wisłok Valley, Southeast Poland (Superson et al., 2010); the Permian in Ulladulla area, in the lower terrace of the Warta River valley, Menyuan Basin, south of the Qilian Mountains (Vandenberghe et al., 2016); the Sydney Basin, Australia (Du and Yu, 2017); and Central Poland (Petera-Zganiacz and Dzieduszyńska, 2017).

4.5 Clastic dykes

Clastic dykes refer to the veins within unconsolidated deposits, in which liquefaction and/or fluidization cause a sand layer to intrude into an adjacent sedimentary layer (Qiao et al., 2017). Clastic dykes are observed in the DC–2 section, at depths of 0.2–3.6 m (Fig. 7). The parent material of the dyke is a sand layer. The dyke is characterized by columnar sand ejected into the overlying debris gravel sediments. Meanwhile, the upward–flowing sand and clayey silt also entrained the surrounding gravel as it was ejected into the upper sediments, forming the sausage morphology structure. A typical clastic dyke is 1–4 m wide and 0.5–3.4 m high. Liquefied veins are observed in the DC–3 section, at depths of 3–4.5 m, and are overlain and underlain by gravel beds (Fig. 10). The liquified sand or clayey silt intrudes upwards into the overlying gravel layer, it is then affected by gravity loading, which causes subsequent lateral flow and

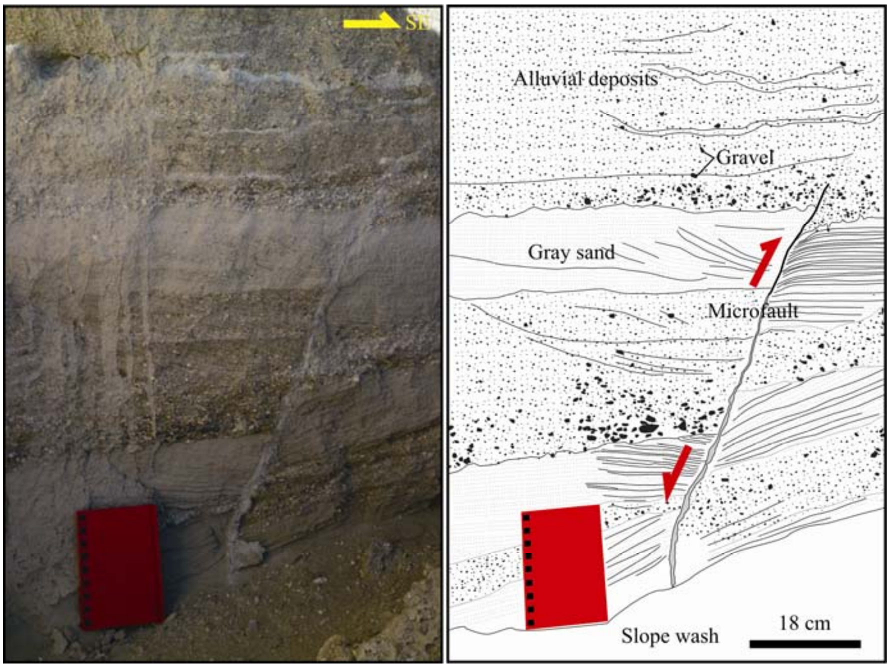

Fig. 5. Micro–faults and sand dyke in the DC–1 alluvial deposits section. Note the lithology and bedding changes in the strata on both sides of the fault. Notebook (18 cm long) for scale (similar for Figs. 8b, 8c).

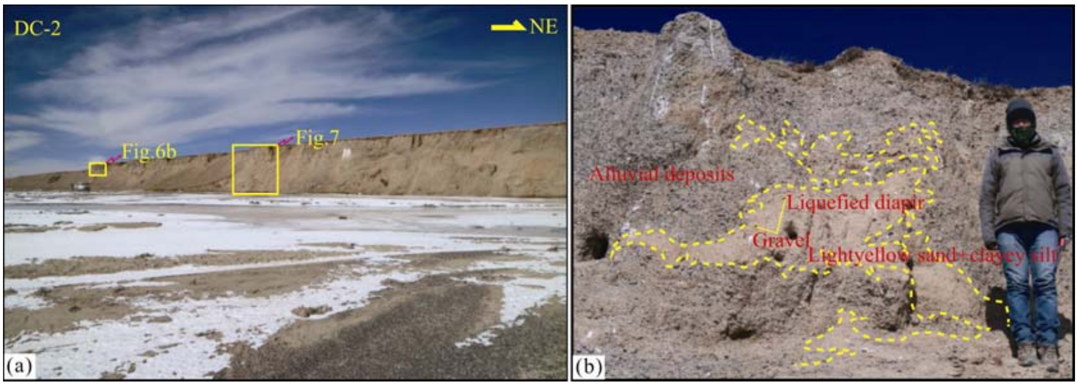

Fig. 6. Liquefied diapir or an irregular injection in the DC–2 alluvial deposits section. Person (170 cm high) for scale.

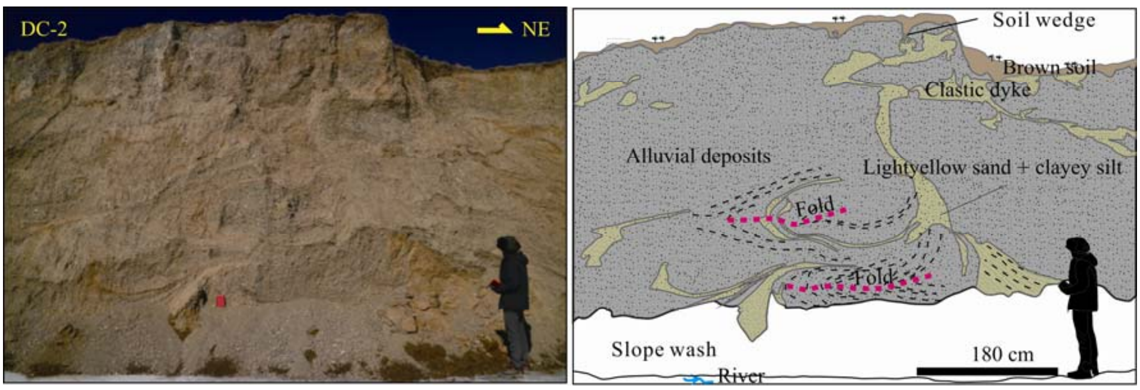

Fig. 7. Recumbent folds (sand layer and gravel layer are bent and deformed; also note the fold axial changes) and clastic dykes (liquefaction deformation of the sand layer, and lateral flow in the parent rock layer with parallel bedding) in the DC–2 alluvial deposits section. Person (180 cm high) for scale (similarly for Figs. 8−10).

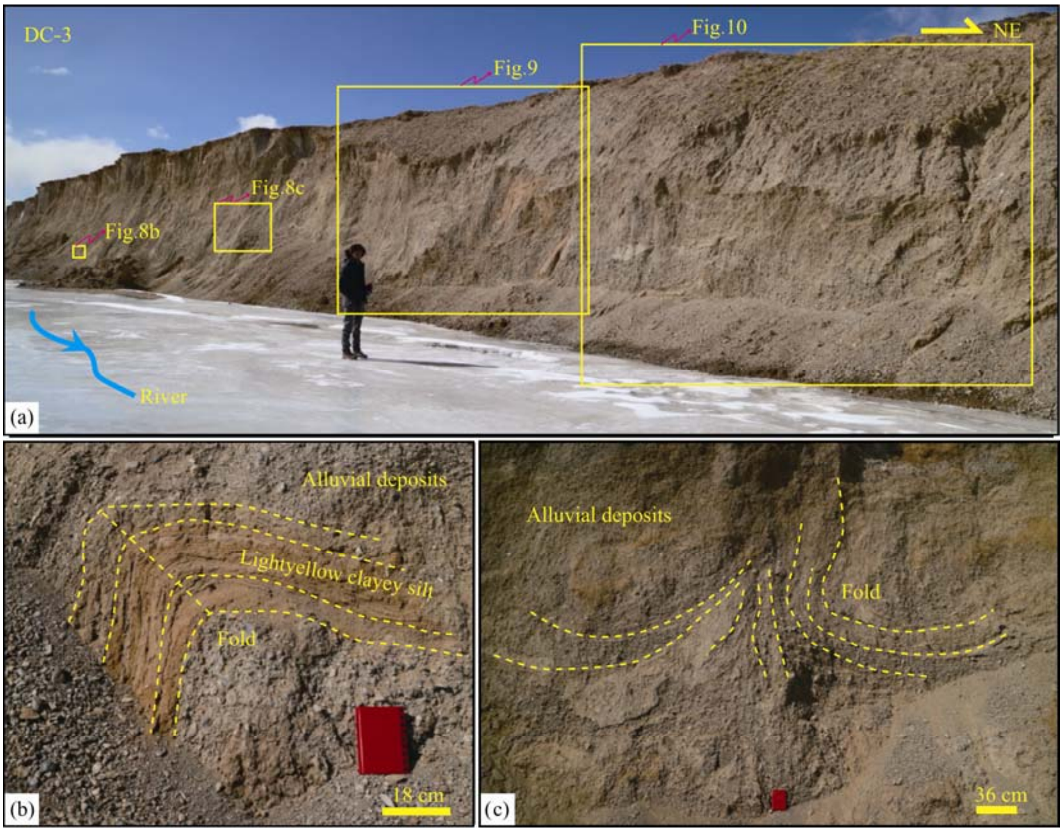

Fig. 8. Irregular folds in the DC–3 alluvial deposits section.
(a) Location and distribution of SSDS in the DC-3 profile; (b) the light yellow clayey silt layer is bent and deformed, overlain and underlain by gravel layers; (c) the sand layer and the gravel layer are bent and deformed to form a fold. Note the orientation of the gravel.

deformation. The original layer eventually disappears, forming irregular, blind veins. The deformation structure is 0.1–1.6 m wide and 0.1–1 m high.

Similar deformational structures have been described on the east flank of the proglacial braided plain of Solheimajokull, southern Iceland (Heron and Etienne, 2005); the glacial sand-sheet deposits in the Tuktoyaktuk Coastlands, western Arctic Canada (Murton and Bateman, 2007); the Aizvejas sand quarry, comprising subglacial bedforms of the Zemgale Ice Lobe, south-eastern Baltic (Lamsters and Zelcs, 2015), the upper part of the Liantuo Formation of the Shennongjia at the northern margin of the Yangtze Craton (Wang et al., 2018).

5 Discussion

5.1 Triggering Mechanism of the SSDS

Owing to the alluvial depositional environment of the DC outcrop presented here, possible triggering mechanisms for these SSDS are: (1) flood, (2) channel erosion, (3) rapid sedimentation and overloading, (4) near-surface gravity slides, (5) rapid groundwater movement, (6) earthquakes, and (7) freeze/thaw cycles.

The deformation structures in flood sediments have parallel sandy layers, a distinct grain sequence and a deformation magnitude that decreases downwards in the vertical section (Rana et al., 2016). In the DC section, deformation structures present no changes in vertical extent or grain sequence, and the lithology primarily comprises poorly-sorted gravel and sand. In addition, sand flows associated with water seeping beneath levees during floods, which have tubular structures, fine and well-sorted grain sizes, and are always located near-surface (as described by Li et al., 1996), were not found. The diapirs or flame-like structures in this study contrast with the concave–upwards, inclined bedding and channel erosional morphologies (recumbent flame structures and asymmetric load casts) described by Dasgupta (1998). Additionally, evidence of rapid sedimentation (Lowe, 1975) and overloading (Moretti and Sabato, 2007; Owen and Moretti, 2008) is absent. Consequently, flooding, channel erosion and rapid sedimentation and overloading, respectively, can be discarded as potential triggers.

In the lower deformed bedding of the DC–2 and DC–3 sections (Figs. 4, 6, 7), fold structures with deformed sand and gravel layers might have been triggered by near–surface gravity slides; however, the axial directions of these folds are directed upstream of the river, which is opposite to the direction of stress caused by cryoturbation or alluvial fan gravity slides along the slope. In the DC section, there is no obvious sliding surface in the SSDS, and also a lack of the typical structures of the extensional zone (normal faults), shear zone (monoformal folds) and compressional zone (folds and thrusts) of slump folds

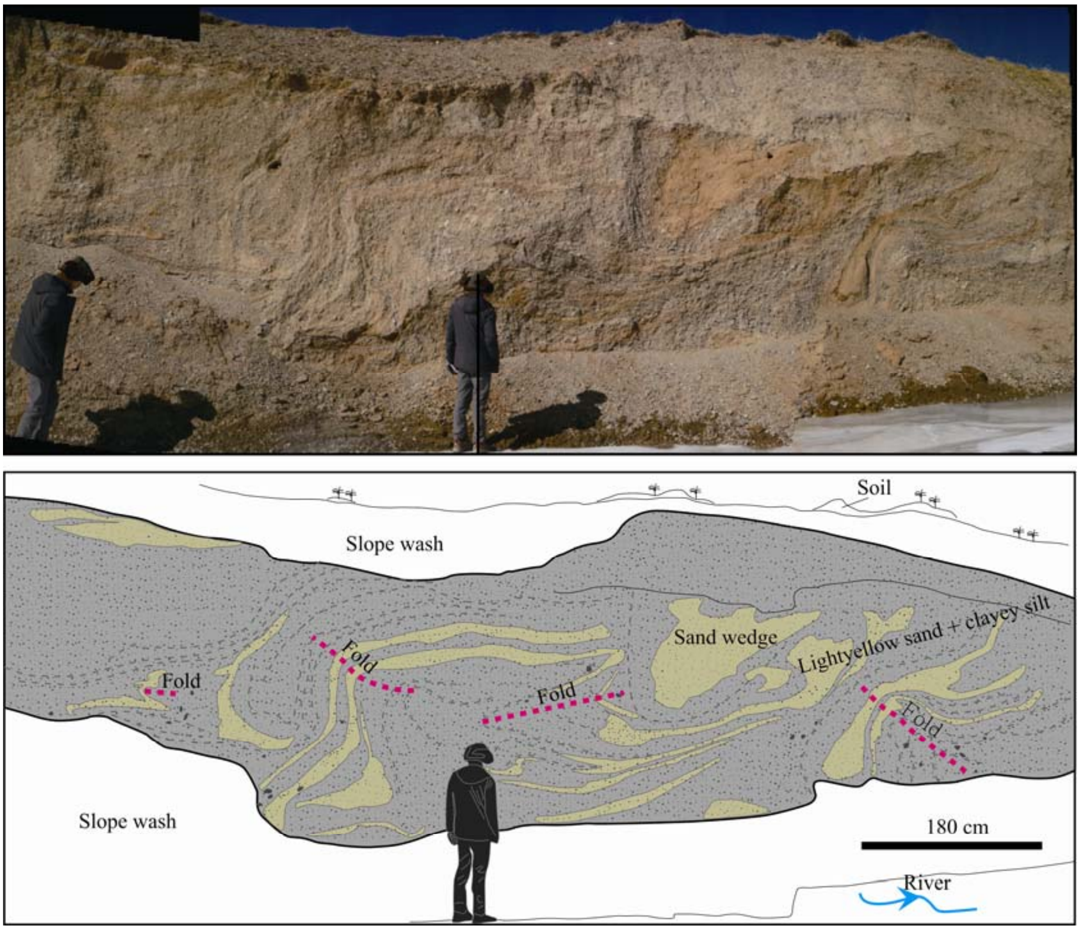

Fig. 9. Folds and sand wedges in the DC–3 alluvial deposits section. Note changes in the fold axis and strata.

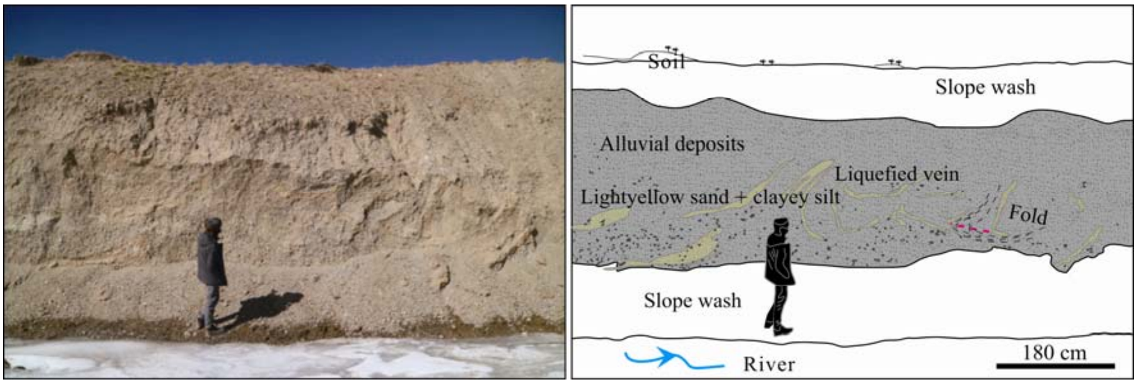

Fig. 10. Liquefied veins (mainly blind veins without roots) and recumbent folds in the DC–3 alluvial deposits section.

(Alsop and Marco, 2011; Lü et al., 2011; Yang and Van Loon, 2016; Qiao et al., 2017). Furthermore, the slope of the low–inclination Changshui alluvial fan (dip <1°) is too low to create shear parallel to the sediment surface as observed in the deformed DC section (see Moretti et al., 2001). The clastic dykes and fold structures in the DC section are obviously different from typical structures (macro-scale turbate structures with matrix core or stone core, clast reorientations following a recumbent fold, vertically realigned clasts along a water-escape pipe) that were induced by porewater pressure controls on subglacial sediments (Ravier et al., 2014).

As often emphasized (e.g. Du and Yu, 2017), it is important but usually difficult to distinguish seismic and aseismic SSDS in Quaternary deposits. Therefore, we compare the main characteristics and formation processes of SSDS associated with seismic and freeze/thaw cycles (see Table 1). As described above, the DC section is located close to the F1 fault. While the SSDS (except micro–faults) in this study may have been induced by earthquakes, we propose instead that these structures were caused by freeze/thaw cycles for five reasons as follow.

Table 1 Selected deformation structures attributed to freeze–thaw cycles and seismic processes (modified from Collins, 2015)

Freeze–thaw cycles		Seismic	
Form	Process and key features	Form	Process and key features
Sand or soil wedge	Freeze expansion and then gravity driven (i.e. downwards) infilling of a thermal contraction or mass movement induced fissure. Typically wider at top. May show stratification.	Colluvial wedge	A fault is displaced to form a fault cliff, a wedge–shaped deposit is then formed by erosion (gravity and/or water). Particles close to the fault are coarse; particles further away are fine and often have no bedding.
Diapir	Slight plastic deformation under the compressive stress or pore fluid pressure drives upwards or lateral movement of un–liquefied or liquefied sediments, such that they puncture through overlying layers. May cause regular bending deformation of the overlying layer.	Liquefied diapir	Plastic upwards deformation under seismic load stress or pore fluid pressure drives liquefied sediments to puncture through overlying layers (principally upwards). Grades into injection dykes, if sand/sediment becomes fully liquefied. Reflects deeper unit having a lower dynamic viscosity than overlying sand/sediment.
Fold	Pore fluid pressure and gravity collapse due to the changes in pore water and volume of sediment after ice meltscause plastic deformation of sediments. Mostly symmetrical folds, and the pleated axial surface has a preferred orientation. May show preferred particle orientation.	Hydraplastic fold	Pore fluid pressure causes plastic sediment deformation under seismic shear stress. The sediments are continuously bent but not cracked.
Clastic dykes	Pore fluid pressure or gravity collapse drives clastic sediments upwards or laterally. Parent sediment fabric is lost.	Liquefied dykes	Pore fluid pressure drives vertical flow (up or down) of liquefied sediments. They generally cut through horizontal beds as inclined to vertical conduits. The dykes are often bent and deformed, and connected to the mother rock deposits.

(1) The DC section is located in the northern Qiangtang Basin, with an average elevation of 4800 m, and the annual average temperature is below 0°C. Permafrost (Yang et al., 2003; Wang et al., 2003; Wang et al., 2015), snowbergs, frost mounds and gelifluction are widely distributed, resulting in typical periglacial landforms. (2) Cryogenic wedges and fissures typically develop in periglacial environments (Harry and Goździk, 1988). The deformed structures are concentrated at depths of 1–5 m below the surface. (3) The symmetrical arrangement of layers on both sides of the fold structures, and the lack of characteristic fillings, excludes tension wedges (van Vliet–Lanoëet al., 2000, 2004). (4) These SSDS are non–interlayered, have a meter deformation scale, are most commonly within unlithified deposits, and have a largely inhomogeneous lithology (Table 2). (5) The deformation structures are consistent with plastic deformation, in a–low speed and low–pressure movement of loose deposits (Table 2). These SSDS described here are obviously different from those attributed to liquefaction or fluidization deformation (centimeter scale, interlayered, high–speed, high–pressure and fast fluid deformation) caused by earthquakes (Table 2).

5.2 SSDS Processes

Freeze/thaw cycles is an effective mechanism for generating SSDS, especially in periglacial settings (Peterson et al., 2003). Freeze/thaw cycles can cause freeze expansion and thermal contraction, potentially generating high pore pressures, resulting not only in fluidization of the sediments but also in injection (Vandenberghe, 2007). Moreover, cryostatic pressures and frost disturbance of the sediments occur randomly; therefore, they should result in irregularly spaced structures (Vandenberghe, 2007). The main sedimentary processes related to freeze/thaw cycles in the DC section are freeze-melt out, re-sedimentation and SSDS. The original undeformed layer (from bottom to top) comprises: permafrost, active layer (thaw) and overlying layer (Fig.11a). Some original cracks may occur on the surface of the permafrost layer. During the freezing phase (Fig.11b), pore water in the active layer begins to freeze, raising cryostatic pressure and resulting in sediment volume expansion. Due to the upwards compressive stress, the top sediments of the active layer form an upwards diapirs, resulting in bending deformation of the overlying layer and possibly forming new cracks. These cracks are filled with ice and gradually enlarge, eventually forming larger cryogenic wedges. The expansion of the sediments causes upwards and lateral compression stresses, causing the particles in the active layer to be dislocated or displaced, result in a bedding dislocation (micro–fault) or disturbance deformation. During the thawing phase (Fig.11c), ice in the active layer begins to melt and the sediment volume shrinks (because of thermokarst processes). The sediments gradually become supersaturated and the pore water pressure increases. The bottom of the water–saturated sediment has a high pore pressure, causing liquefaction and/or fluidization, and leading to upwards or lateral sediment movement and the formation of liquefied veins and clastic dykes. Liquefaction and/or fluidization, and gravitational loading-induced sediment collapse, will cause the water–saturated sediment to bend and fold. Due to the low pressure and slow deformation, we can observe a directional gravel arrangement and symmetrical folds. During gravitational

Table 2 The different deformation structures attributed to freeze–thaw cycles and seismic processes

	Freeze–thaw cycles	Seismic processes
Distribution	In arctic and high–altitude periglacial setting	Near or along the seismically active belts
Lithology	Gravel, sand, silt, mud and soil; heterogeneous lithology	Fine sand, silt and silty–clay, water–saturated, liquefied sediments
Deformation layer and scale	Non–interlayered deformation and meterscale	Interlayered deformation and centimeter or decimetrescale
Deformation feature	In–situ, low–speed and low–pressure movement of loose deposits, and mostly plastic deformation	In–situ or flow, high–speed and high–pressure fluid movement; mostly liquefaction or fluidization deformation
Trigger stress	Cryostatic pressure, gravitational loading and thermokarst	Seismic shear force (such as Raleigh wave)
Influential factor	Temperature, hydrothermal changes in the soil	Earthquake magnitude and distance from the epicenter

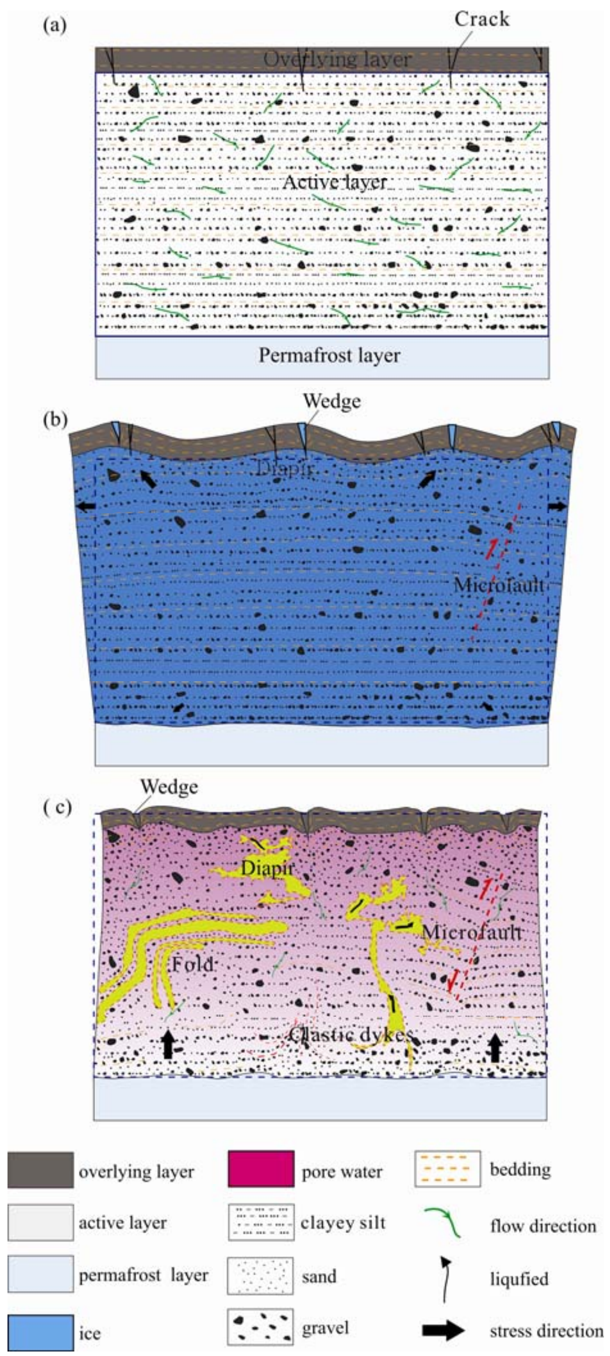

Fig. 11. Schematic of the formation process of SSDS in the DC section.

(a) The original undeformed layer; (b) in freezing phase, some ice wedges appear in the top sediments, due to cryostatic pressure; (c) in thawing phase, the water–saturated sediments begin to liquefy and/or fluidize to form liquefied diapirs, liquefied veins and clastic dykes under the super-porosity water pressure. Due to gravitational loading, water–saturated sediments are disturbed and deformed to form folds. Dislocations and sediment particle disturbances occur in the formation.

collapse, the sediment particles are dislocated or displaced again, and the original bedding pattern gradually disappears. With changing temperature and hydrothermal conditions, sediments undergo successive freeze/thaw cycles, resulting in large and diverse deformation structures. These can reflect the slow, long–term repeated freeze/thaw cycles.

Under the background of global warming, the permafrost on the TP will shrink, leading to more intense freeze/thaw cycles across wider regions (Wang et al., 2014), and a greater number of SSDS. Furthermore, melting of ground ice near the permafrost table produces uneven thaw settlement and freeze/thaw cycles in the active layer, posing a significant threat to infrastructure and engineering constructions over permafrost (Nelson et al., 2001, Ma et al., 2009; Ma et al., 2017). Therefore, the safety of traffic engineering and pipeline construction must take into account volume changes which occur in frozen ground (Burt and Williams, 1976). The freeze/thaw cycles and SSDS in permafrost regions should be seriously considered.

6 Conclusions

Based on the soft–sediment deformation structures (SSDS) in three well–exposed alluvial outcrops near Dogai Coring, northern Qiangtang Basin, integrated with the geographic setting, lithology and deformation features, we draw three conclusions summarized briefly as follows.

(1) Four types of SSDS (diapirs, clastic dykes, folds and cryogenic wedges) were identified, all characterized by meter–scale, non–interlayered, low–speed and low–pressure displacements within soft sediments, most commonly in the form of plastic deformation. These SSDS can be interpreted as resulting from freeze/thaw cycles, reflecting the regional climate changes and fluctuations of hydrothermal conditions in the soil.

(2) Micro–faults are associated with regional fault activity; however, we were unable to identify the nature of the micro–faults, perhaps due to volume expansion and gravity collapse during subsequent freeze/thaw cycles.

(3) This study helps us to recognize the differences between deformation structures attributed to freeze/thaw cycles and those attributed to seismic processes.

Acknowledgements

During this study, the authors carefully read the book “Soft sedimentary deformation structures-earthquake and ancient earthquake records” by Qiao Xiufu et al., 2017, which has greatly helped us to understand, assess and interpret the soft sedimentary deformation structures in the area. We thank Drs. Qiao Xiufu, Su Dechen, Pan Jiawei, He Xiangli and Chen Andong for their fruitful discussion. We are also grateful A.J. (Tom) Van Loon for valuable suggestions and the English improvement. This work is supported by projects from the National Natural Science Foundation of China (41807298, 41702372, 41672211), the China Postdoctoral Science Foundation (2019M650788), National Key Research and Development Project of China (2016YFC0600310), the China Geological Survey (DD20160022, DD20190059), and the Basic Research Funds (JYYWF201810) of the Institute of Geology, CAGS.

Manuscript received Feb. 11, 2019

accepted Dec. 20, 2019
associate EIC YANG Jingsui
edited by LIU Lian

References

Alfaro, P., Delgado, J., Estevez, A., and Lopez-Casado, C., 2001. Paleoliquefaction in the BajoSegura Basin (eastern Betic Cordillera). Acta Geologica Hispanica, 36(3): 233–244.

Alfaro, P., Delgado, J., Estévez, A., Molina, J.M., Moretti, M., and Soria, J.M., 2002. Liquefaction and fluidization structures in Messinian storm deposits (Bajo Segura Basin, Betic Cordillera, southern Spain). International Journal of Earth Sciences (Geol. Rudnsch), 91(3): 505–513.

Alsop, G.I., and Marco, S., 2011. Soft-sediment deformation within seismogenic slumps of the Dead Sea basin. Journal of Structural Geology, 33(4): 433–457.

Bertran, P., Allenet, G., Gé, T., Naughton, F., Poirier, P., and Goñi, M.F.S., 2010. Coversand and pleistocene palaeosols in the landes region, southwestern France. Journal of Quaternary Science, 24(3): 259–269.

Burt, T.P., and Williams, P.J., 1976. Hydraulic conductivity in frozen soils. Earth Surface Processes & Landforms, 1(4): 349–360.

Chen, L.J., 2012. Lake level fluctuation and glacier advances in north puruogangri since the middle Holocene. Chinese Academy of Sciences, Beijing, Master thesis, 1–58 (in Chinese).

Collins, P.E., 2015. Active Tectonic Risk Assessment–Problems with Soil and Soft Sediment Deformation Structures. In Engineering Geology for Society and Territory–Volume 6 (pp. 161–165). Springer, Cham.

Dasgupta, P., 1998. Recumbent flame structures in the Lower Gondwana rocks of the Jharia Basin, India-a plausible origin. Sedimentary Geology, 119(119): 253–261.

Du, Y.S., and Yu, W.C., 2017. Earthquake–caused and non–earthquake–caused soft–sediment deformations. Journal of Palaeogeography, 19(1): 65–72 (in Chinese with English abstract).

Ge,Y.Z., Zhong, J.H., Fan, X.F., Ren, Q.Q., and Shao, Z.F., 2015. Study on internal sedimentary and structural features of the slump body in Linshan island, Qingdao, Shandong. Geological Review, 61(3): 634–643 (in Chinese with English abstract).

Giles, D.P., Griffiths, J.S., Evans, D.J.A., and Murton, J.B., 2017. Geomorphological framework: glacial and periglacial sediments, structures and landforms. Geological Society, London, Engineering Geology Special Publications, 28(1): 59–368.

Greb, S.F., and Archer, A.W., 2007. Soft–sediment deformation produced by tides in a meizoseismic area, Turnagain Arm, Alaska. Geology, 35(5): 435–438.

Harry, D.G., and Gozdzik, J.S., 1988. Ice wedges: Growth, thaw transformation, and palaeoenvironmental significance. Journal of Quaternary Science, 3(1): 39–55.

He, B.Z., and Qiao, X.F., 2015. Advances and overview of the study on paleoearthquake events: a review of seismites. Acta Geologica Sinica, (English Edition), 89(5): 1702–1746.

Heron, D.P.L., and Etienne, J.L., 2005. A complex subglacial clastic dyke swarm, sólheimajokull, southern iceland. Sedimentary Geology, 181(1-2): 25–37.

Jiang, H., Zhong, N., Li, Y., Xu, H., Yang, H., and Peng, X., 2016. Soft sediment deformation structures in the Lixian lacustrine sediments, eastern Tibetan Plateau and implications for postglacial seismic activity. Sedimentary Geology, 344: 123–134.

Jin, H.J., Chang, X.L., Luo, D.L., He, R.X., Lü, L.Z., Yang, S.Z., and Guo, Y.D., 2016. Evolution of permafrost in northeast China since the late Pleistocene. Sciences in Cold and Arid Regions, 8(4): 269–296.

Lamsters, K., and Zelcs, V., 2015. Subglacial bedforms of the zemgale ice lobe, south-eastern Baltic. Quaternary International, 386: 42–54.

Liang, L., Dai, F., Jiang, H., and Zhong, N., 2018. A Preliminary Study on the Soft–Sediment Deformation Structures in the Late Quaternary Lacustrine Sediments at Tashkorgan, Northeastern Pamir, China. Acta Geologica Sinica (English Edition), 92(4): 1574–1591.

Li, Y., Wang, C., Dai, J., Xu, G., Hou, Y., and Li, X., 2015. Propagation of the deformation and growth of the Tibetan–Himalayan orogen: A review. Earth–Science Reviews, 143: 36–61.

Li, Y., Craven, J., Schweig, E.S., and Obermeier, S.F., 1996. Sand boils induced by the 1993 Mississippi River flood: Could they one day be misinterpreted as earthquake-induced liquefaction?. Geology, 24(2): 171-174.

Li, Y., Zhong, J.H., Shao, Z.F., and Mao, M., 2012. An overview on the classification and genesis of soft sediment deformation structure. Geological Review, 58(5): 829–838 (in Chinese with English abstract).

Lin, N.F., Shen, W.S., Zhang, H., and Li, H.D., 2012. Correlation degree analysis of meteorological elements and dynamic remote sensing of alpine lakes in Naqu region of Tibet in the past 35 years. Journal of Ecology & Rural Environment, 28 (3): 231–237 (in Chinese with English abstract).

Lü, H.B., Wang, J., and Zhang, H.C., 2011. Discovery of the late Mesozoic slump beds in Linshan island, Shangdong, and a pilot research on the regional tectonics. Acta Geologica Sinica, 85(6): 938–946 (in Chinese with English abstract).

Lowe, D.R., 1975. Water escape structures in coarse grained sediments. Sedimentology, 22: 157–204.

Ma, W., Cheng, G.D., and Wu, Q.B., 2009. Construction on permafrost foundations: lessons learned from the Qinghai–Tibet railroad. Cold Regions Science and Technology, 59(1): 3–11.

Ma, W., Mu, Y.H., Xie, S.B., Mao, Y.C., and Chen, D., 2017. Thermal–mechanical influences and environmental effects of expressway construction on the Qinghai–Tibet permafrost engineering corridor. Advances in Earth Science, 32(5): 459–464 (in Chinese with English abstract).

Massari, F., Ghibaudo, G., D'alessandro, A., and Davaud, E., 2001. Water-upwelling pipes and soft-sediment deformation structures in lower Pleistocene calcarenites (Salento, southern Italy). Geological Society of America Bulletin, 113(5): 545–560.

Mao, F., Lu, Z.G., Zhang, J.H., and Zheng, L.Y., 2007. Analysis on climate characteristics in naqu in recent 40 years. Plateau Meteorology, 26(4): 708–715(in Chinese with English abstract).

Molina, J.M., Alfaro, P., Moretti, M., and Soria, J.M., 1998. Soft-sediment deformation structures induced by cyclic stress of storm waves in tempestites (Miocene, Guadalquivir basin, Spain). Terra Nova, 10: 145–150.

Moretti, M., Soria, J.M., Alfaro, P., and Walsh, N., 2001. Asymmetrical soft–sediment deformation structures triggered by rapid sedimentation in turbiditic deposits (late miocene, guadix basin, southern Spain). Facies, 44(1): 283–294.

Moretti, M., and Sabato, L., 2007. Recognition of trigger mechanisms for soft–sediment deformation in the Pleistocene lacustrine deposits of the Sant􀀀Arcangelo Basin (Southern Italy): Seismic shock vs. overloading. Sedimentary Geology, 196(1–4): 31–45.

Murton, J.B., Whiteman, C.A., and Allen, P., 1995. Involutions in the middle Pleistocene (anglian) barham soil, eastern England: a comparison with thermokarst involutions from arctic Canada. Boreas, 24(3): 269–280.

Murton, J.B., 2001. Thermokarst sediments and sedimentary structures, tuktoyaktuk coastlands, western arctic Canada. Global & Planetary Change, 28(1): 175–192.

Murton, J.B., and Bateman, M.D., 2007. Syngenetic sand veins and anti‐syngenetic sand wedges, tuktoyaktuk coastlands, western arctic canada. Permafrost and Periglacial Processes, 18(1): 33–47.

Nelson, F.E., Anisimov, O.A., and Shiklomanov, N.I., 2001. Subsidence risk from thawing permafrost. Nature, 410(6831): 889–890.

Niu, X.S., Liu, X.F., and Chen, W.X., 2014. Hydrochemical characteristic and origin for salt springs water in Dogai Doring area of north Qiangtang Basin, Tibet. Acta Geologica Sinica, 88(6): 1003–1010 (in Chinese with English abstract).

Obermeier, S.F., 1996. Use of liquefaction–induced features for paleoseismic analysis. An overview of how seismic liquefaction features can be distinguished from other features and how their regional distribution and properties of source sediment can be used to infer the location and strength of Holocene paleo–earthquakes. Engineering Geology, 44(1–4): 1–76.
Owen, G., 1987. Deformation processes in unconsolidated sands. Geological Society, London, Special Publications, 29(1): 11–24.
Owen, G., 1996. Experimental soft-sediment deformation: structures formed by the liquefaction of unconsolidated sands and some ancient examples. Sedimentology, 43: 279–293.
Owen, G., and Moretti, M., 2008. Determining the origin of soft–sediment deformation structures: a case study from Upper Carboniferous delta deposits in south–west Wales, UK. Terra Nova, 20(3): 237–245.
Owen, G., and Moretti, M., 2011. Identifying triggers for liquefaction–induced soft–sediment deformation in sands. Sedimentary Geology, 235(3–4): 141–147.
Pawelec, H., Drewnik, M., and Marcin, Z., 2015. Paleoenvironmental interpretation based on macro- and microstructure analysis of pleistocene slope covers: a case study from the miechów upland, poland. Geomorphology, 232: 145–163.
Petera‐Zganiacz, J., and Dzieduszyńska, D.A., 2017. Palaeoenvironmental proxies for permafrost presence during the Younger Dryas, central Poland. Permafrost and Periglacial Processes, 28(4): 726–740.
Peterson, R.A., Walker, D.A., Romanovsky, V.E., Knudson, J.A., and Raynolds, M.K., 2003. A different frost heave model: cryoturbation vegetation interactions. In: Phillips M, Springmann SM, Arenson LU (eds) Permafrost: proceedings of the 8th international conference on Permafrost: proceedings of the 8th international conference on Permafrost, Zurich, Switzerland, 21–25 July 2003, pp 885–890.
Petersen, J., Wilhelm, B., Revel, M., Rolland, Y., Crouzet, C., Arnaud, F., Brisset, E., Chaumillon, E., and Magand, O., 2014. Sediments of Lake Vens (SW European Alps, France) record large-magnitude earthquake events. Journal of Paleolimnology, 51(3): 343–355.
Postma, G., 1983. Water escape structures in the context of a depositional model of a mass flow dominated conglomeratic fan-delta (Abrioja Formation, Pliocene, Almeria Basin, SE Spain). Sedimentology, 30(1): 91–103.
Qiao, X.F., Li, H.B., Su, D.C., He, B.Z., Tian, H.S., Guo, X.P., Song, T.R., Lü, H.B., Gao, L.Z., He, J., Yuan, X.Q., Zhou, W., Zhang, M., Sun, A.P., and Wang, A.D., 2017. Soft–sediment deformation structures–earthquakes and seismic records. Beijing: Geological Publishing House, 1–264 (in Chinese).
Rana, N., Sati, S.P., Sundriyal, Y., and Juyal, N., 2016. Genesis and implication of soft–sediment deformation structures in high–energy fluvial deposits of the Alaknanda Valley, Garhwal Himalaya, India. Sedimentary Geology, 344: 263–276.
Ratschbacher, L., Krumrei, I., Blumenwitz, M., Staiger, M., Gloaguen, R., Miller, B.V., Samson, S.D., Edwards, M. A., and Appel, E., 2011. Rifting and strike–slip shear in central Tibet and the geometry, age and kinematics of upper crustal extension in Tibet. Geological Society London Special Publications, 353(1): 127–163.
Ravier, E., Buoncristiani, J.F., Guiraud, M., Menzies, J., Clerc, S., Goupy, B., and Portier, E., 2014. Porewater pressure control on subglacial soft sediment remobilization and tunnel valley formation: a case study from the Alnif tunnel valley (Morocco). Sedimentary Geology, 304: 71–95.
Ren, Z.L., Cui, J.P., Liu, C.Y., Li, T.J., Chen, G., Dou, S., Tian, T., and Luo, Y.T., 2105. Apatite fission track evidence of uplift cooling in the Qiangtang Basin and constraints on the Tibetan Plateau Uplift. Acta Geologica Sinica (English Edition), 89 (2): 467–484.
Rodríguez-López, J.P., Meléndez, N., Soria, A.R., Liesa, C.L., and Van Loon, A.T., 2007. Lateral variability of ancient seismites related to differences in sedimentary facies (the synrift Escucha Formation, mid-Cretaceous, eastern Spain). Sedimentary Geology, 201(3-4): 461–484.
Superson, J., Gębica, P., and Brzezińska–Wójcik, T., 2010. The origin of deformation structures in periglacial fluvial sediments of the Wisłok valley, southeast Poland. Permafrost and Periglacial Processes, 21(4): 301–314.
Tian, H.S., Zhang, Z.Q, Zhang, B.H., Zhu, J.W., Sang, Z.X., and Li, H.K., 2013. Tectonic taphrogenesis and paleoseismic records from the Yishu fault zone in the initial stage of the caledonian movement. Acta Geologica Sinica (English Edition), 87(4): 936–947.
Tian, H.S., Zhang, S.H., and Zhang, A.S., 2016. Test investigation on liquefied deformation structure in saturated lime–mud composites triggered by strong earthquakes. Acta Geologica Sinica (English Edition), 90(6): 2008–2021
Van Loon, A.J., and Brodzikowski, K., 1987. Problems and progress in the research on soft–sediment deformations. Sedimentary Geology, 50(1–3):167–193.
Van Loon, A.J., 2009. Soft-sediment deformation structures in siliciclastic sediments: an overview. Geologos, 15 (1):3-55.
Van Vliet–Lanoë, B., Meilliez, F., Laurent, M., and Mansy, J.L., 2000. Neotectonic and seismic activity in the English Channel and Dover Strait: the differentiation between co–seismic and periglacial deformations. Potential for large earthquakes in low seismic activity regions of Europe. Han. Han/Lesse Cahiers du Centre Européen de Géodynamique et de Séismologie, 18: 163–165.
Van Vliet–Lanoë, B., Magyari, A., and Meilliez, F., 2004. Distinguishing between tectonic and periglacial deformations of Quaternary continental deposits in Europe. Global and Planetary Change, 43(1–2): 103–127.
Vandenberghe, J., 1988. Cryoturbations. In: Clark, M.J. (Ed.), Advances in Periglacial Geomorphology. John Wiley and Sons, Chichester, pp. 179–198.
Vandenberghe, J., 1992. Cryoturbations: a sediment structural analysis. Permafrost & Periglacial Processes, 3(4): 343–351.
Venberghe, J., Cui, Z., Zhao, L., and Zhang, W., 2004. Thermal‐contraction‐crack networks as evidence for late‐pleistocene permafrost in inner mongolia, china. Permafrost & Periglacial Processes, 15(1): 21–29.
Vandenberghe, J., 2007. Periglacial landforms/cryoturbation structures. Encyclopedia of Quaternary Science, 3(4): 2147–2153.
Venberghe, J., Cui, Z., Zhao, L., and Zhang, W., 2014. Thermal‐contraction‐crack networks as evidence for late‐Pleistocene permafrost in inner Mongolia, China. Permafrost & Periglacial Processes, 15(1): 21–29.
Vandenberghe, J., Wang, X., and Vandenberghe, D., 2016. Very large cryoturbation structures of Last Permafrost Maximum age at the foot of the Qilian Mountains (NE Tibet Plateau, China). Permafrost and Periglacial Processes, 27(1): 138–143.
Wang, J.S., Zhang, X.Z., Zhao, Y.P., Shen, Z.X., Shi, P.L., and Yu, C.Q., 2008. Spatio–temporal Pattern of Climate Changes in Northern Tibet's Qiangtang Plateau. Resources Science, 30 (12): 1852–1859.
Wang, C.H., Dong, W.J., and Wei, Z.G., 2003. A study on relationship between freezing thawing processes of the Qinghai–Xizang plateau and the atmospheric circulation over east Asia. Chinese Journal of Geophysics, 46(3): 438–448 (in Chinese with English abstract).
Wang, C.H., Jin, S.L., and Shi, H.X, 2014. Area change of the frozen ground in china in the next 50 years. Journal of Glaciology & Geocryology, 36(1): 1692–1696 (in Chinese with English abstract).
Wang, C.S., Li, Y.L., and Li, Y.T., 2006. Discussion on evaluation of oil and gas resources in Qinghai–Tibet plateau. Acta Petrolei Sinica, 27: 1–7 (in Chinese with English abstract).
Wang, P.K., Zhu, Y.H., Zhang, X.H., Zhang, S, Pang, S.J., Xiao, R., and Li, B., 2015. Permafrost structures and their effects on the accumulation of the natural gas hydrates in the Qiangtang Basin, northern Xizang. Sedimentary Geology & Tethyan Geology, 35: 57–67 (in Chinese with English abstract).
Wang, H.A., Zhong, J.H., Chen, X., and Gao, Y.F., 2008.Characteristics of Cretaceous seismite in the Tamuchage depression, Mongolia, and its significance. Acta Geologica Sinica, 82(6): 1088–1095 (in Chinese with English abstract).

Wang, Y.C., Kuang, H.W., Peng, N., Liu, Y.Q., Fan, Z.X., Xia, X.X., Chen, X.S., Zheng, X.M., and Sun, Y.X., 2018. Freezing and thawing structures: An evidence of cold climate in the Neoproterozoic Liantuo Fotmation of the Shennongjia in the northern margin of the Yangtze Craton. Journal of Palaeogeography, 20(4): 579–594 (in Chinese with English abstract).

Wang, P., Zhang, B., Qiu, W.L., and Wang, J.C., 2011. Soft–sediment deformation structures from the Diexi paleo–dammed lakes in the upper reaches of the Minjiang River, east Tibet. Journal of Asian Earth Sciences, 40(4): 865–872.

Wang, X., Vandenberghe, D., Yi, S., Vandenberghe, J., Lu, H., Van Balen, R., and Van den Haute, P., 2013. Late Quaternary paleoclimatic and geomorphological evolution at the interface between the Menyuan Basin and the Qilian Mountains, northeastern Tibetan Plateau. Quaternary Research, 80(3): 534–544.

Xu, H.Y., Jiang, H.C., Yu, S., Yang, H.L., and Chen, J., 2015. OSL and pollen concentrate 14C dating of dammed lake sediments at Maoxian, east Tibet, and implications for two historical earthquakes in AD 638 and 952. Quaternary International, 371: 290–299.

Yang, H.T., Li, C., and Li, Q., 2009. Evidence of tectonic activities happened since the Middle Pleistocene in central Qiangtang, northern Tibet, China. Geological Bulletin of China, 28(9):1325–1329 (in Chinese with English abstract).

Yang, M.X., Yao, T.D., Gou, X.H., Koike, T., and He, Y.Q., 2003. The soil moisture distribution, thawing–freezing processes and their effects on the seasonal transition on the Qinghai–Xizang (Tibetan) Plateau. Journal of Asian Earth Sciences, 21 (5): 457–465 (in Chinese with English abstract).

Yang, R., and Van Loon, A.J., 2016. Early Cretaceous slumps and turbidites with peculiar soft-sediment deformation structures on Lingshan Island (Qingdao, China) indicating a tensional tectonic regime. Journal of Asian Earth Sciences, 129: 206–219.

Yang, R., Fan, A., Han, Z., and Van Loon, A.J., 2017. Lithofacies and origin of the late triassic muddy gravity-flow deposits in the ordos basin, central china. Marine and Petroleum Geology, 85: 194–219.

Zhong, N., 2017. Earthquake and Provenance Analysis of the Lacustrine Sediments in the Upper Reaches of the Min River during the Late Pleistocene. Institute of Geology, China Earthquake Administration, Beijing, Doctoral thesis: 1–181 (in Chinese).

Zhong, N., Jiang, H.C., Liang, L.J., Xu, H.Y., and Peng, X.P., 2017. Paleoearthquake researches via soft sediment deformation of load, ball–and–pillow structure: a review. Geological Review, 63(3): 719–738 (in Chinese with English abstract).

Zhong, N., Jiang, H.C., Li, H.B., Xu, H.Y., Shi, W., Zhang, S.Q. and Wei, X.T., 2019. Last Deglacial Soft–Sediment Deformation at Shawan on the Eastern Tibetan Plateau and Implications for Deformation Processes and Seismic Magnitudes. Acta Geologica Sinica (English Edition), 93(2): 430–450.

Zhong, N., Jiang, H.C., Li, H.B., Xu, H.Y., and Huang, X.L., 2020. The Genetic Types of Soft Sediment Deformation Structures and Their Characteristics in the Fluvial-lacustrine Sediments, Eastern Tibetan Plateau. Acta Geoscientica Sinica, 41(1): 23–36 (in Chinese with English abstract).

Zhong, J.H., Cao, M.C, Ni, L.T., Sun, N.L., Liu, C, Hao, B., Yang, G.Q., Song, G.X., and Ge, Y.Z., 2018. Situation of study and development tendency of sand dykes. Journal of Palaeogeography, 20(1): 119–132 (in Chinese with English abstract).

Zieliński, P., Sokołowski, R.J., Woronko, B., Fedorowicz, S., Jankowski, M., and Standzikowski, K., 2016. Sandy deposition in a small dry valley in the periglacial zone of the last glacial maximum: a case study from the józefów site, SE Poland. Quaternary International, 399: 58–71.

About the first author

ZHONG Ning, male, born in 1986 in Henan Province; Graduated from Institute of Geology, China Earthquake Administration. Doctor ZHONG Ning is currently a postdoctor at the Institute of Geology, Chinese Academy of Geological Science. His current research interest focuses on the Active tectonics, paleoearthquake and Soft–sediment Deformational Structures. Email: zdn2018@126.com; phone: 010-68990581.

About the corresponding author

LI Haibing, male, born in 1966 in Anhui Province; doctor; graduated from Institute of Geology, Chinese Academy of Geological Sciences. He is now interested in the study on tectonic geomorphology and paleoearthquake. Email: lihaibing06 @163.com; phone: 010-68990581.